ORIGINAL ARTICLE

Exploring the nigrostriatal and digestive interplays in Parkinson's disease using dynamic total-body [11C]CFT PET/CT

Mei Xin[1] · Yihan Wang[2] · Xinlan Yang[2] · Lianghua Li[1] · Cheng Wang[1] · Yue Gu[2] · Chenpeng Zhang[1] · Gang Huang[1,3] · Yun Zhou[2] · Jianjun Liu[1]

Abstract

Purpose Dynamic total-body imaging enables new perspectives to investigate the potential relationship between the central and peripheral regions. Employing uEXPLORER dynamic [11C]CFT PET/CT imaging with voxel-wise simplified reference tissue model (SRTM) kinetic modeling and semi-quantitative measures, we explored how the correlation pattern between nigrostriatal and digestive regions differed between the healthy participants as controls (HC) and patients with Parkinson's disease (PD).

Methods Eleven participants (six HCs and five PDs) underwent 75-min dynamic [11C]CFT scans on a total-body PET/CT scanner (uEXPLORER, United Imaging Healthcare) were retrospectively enrolled. Time activity curves for four nigrostriatal nuclei (caudate, putamen, pallidum, and substantia nigra) and three digestive organs (pancreas, stomach, and duodenum) were obtained. Total-body parametric images of relative transporter rate constant (R_1) and distribution volume ratio (DVR) were generated using the SRTM with occipital lobe as the reference tissue and a linear regression with spatial-constraint algorithm. Standardized uptake value ratio (SUVR) at early (1–3 min, $SUVR_{EP}$) and late (60–75 min, $SUVR_{LP}$) phases were calculated as the semi-quantitative substitutes for R_1 and DVR, respectively.

Results Significant differences in estimates between the HC and PD groups were identified in DVR and $SUVR_{LP}$ of putamen (DVR: 4.82 ± 1.58 vs. 2.58 ± 0.53; $SUVR_{LP}$: 4.65 ± 1.36 vs. 2.84 ± 0.67; for HC and PD, respectively, both $p < 0.05$) and $SUVR_{EP}$ of stomach (1.12 ± 0.27 vs. 2.27 ± 0.65 for HC and PD, respectively; $p < 0.01$). In the HC group, negative correlations were observed between stomach and substantia nigra in both the R_1 and $SUVR_{EP}$ values ($r=-0.83$, $p < 0.05$ for R_1; $r=-0.94$, $p < 0.01$ for $SUVR_{EP}$). Positive correlations were identified between pancreas and putamen in both DVR and $SUVR_{LP}$ values ($r = 0.94$, $p < 0.01$ for DVR; $r = 1.00$, $p < 0.001$ for $SUVR_{LP}$). By contrast, in the PD group, no correlations were found between the aforementioned target nigrostriatal and digestive areas.

Conclusions The parametric images of R_1 and DVR generated from the SRTM model, along with $SUVR_{EP}$ and $SUVR_{LP}$, were proposed to quantify dynamic total-body [11C]CFT PET/CT in HC and PD groups. The distinction in correlation patterns of nigrostriatal and digestive regions between HC and PD groups identified by R_1 and DVR, or SUVRs, may provide new insights into the disease mechanism.

Keywords Total-body PET/CT · Parkinson's disease · Nigrostriatal-digestive interplays · [11C]CFT · Parametric imaging

---

Mei Xin and Yihan Wang contribute equally to the article.

✉ Yun Zhou
yun.zhou@united-imaging.com

✉ Jianjun Liu
nuclearj@163.com

1 Department of Nuclear Medicine, Ren Ji Hospital, Shanghai Jiao Tong University School of Medicine, 160 Pujian Road, Shanghai 200127, China

2 Central Research Institute, United Imaging Healthcare Group Co, Ltd, 2258 Chengbei Road, Shanghai 201807, China

3 Shanghai Key Laboratory of Molecular Imaging, Shanghai University of Medicine and Health Sciences, Shanghai 201318, China

Introduction

Parkinson's disease (PD) is a progressive neurodegenerative disorder common among the elderly population. The principal pathophysiological change of the disease lies in the depletion of nigrostriatal dopaminergic neurons, leading to a series of motor symptoms including bradykinesia, tremor, rigidity and gait instability [1]. With a broadened understanding of the disease timeline, the integrity of the organism and the interactions between the central and peripheral nerve systems, particularly in relation to the digestive organs, received rising attention [2]. Recent studies proposed that the communication between the brain and digestive systems may be mediated by certain agents that, present in both areas, potentially influence the disease occurrence, development, and modulation [3].

Dopamine transporter (DAT), a neurotransmitter protein on the presynaptic membrane, is responsible for the reuptake of extracellular dopamine (DA) from the synaptic cleft and regulating the DA neurotransmission and homeostasis. Besides the nigrostriatal pathway within the brain, the expression of DAT can also be found at several peripheral sites [4, 5]. Immunohistochemical and in situ hybridization studies have indicated that DATs are abundantly expressed in digestive organs, including the two important nerve branches -- Meissner's and Auerbach's plexuses of the enteric nerve system (ENS), gastric parietal cells and mucosal blood vessel endothelia, duodenal lamina propria, and pancreatic excreting ducts and islets [6–9]. Further to being closely associated with motor dysfunctions in PD, DAT deficits can also lead to anomalies in ENS architecture together with gastrointestinal dysmotility [10, 11]. Several studies have also demonstrated the association between the striatal DAT binding and the activities of gut microbes, suggesting potential DAT modulations in both the central and peripheral regions [12, 13].

However, few suitable approaches were so far available to make a systemic and quantitative analysis of the DAT kinetic distribution in both the central and peripheral organs of human. Nowadays, with the visualization of the imaging biomarkers, progress has been made to understand the etiology of neurodegenerative diseases at molecular level. ^{11}C-2-beta-carbomethoxy-3-beta-(4-fluorophenyl)tropane ($[^{11}C]$CFT), a DAT PET imaging agent commonly used in brain imaging for the diagnosis of PD [14–16], may serve as a potential tracer candidate for its high affinity and selectivity to DAT [17–19] and its resistance to metabolic degradation [20]. Moreover, in animal models, highly specific uptakes of DAT radioligand $[^{18}F]$CFT have been demonstrated in both the striatum and pancreas with the treatment of selective DAT antagonist [19], showing the potential of radionuclide-labeled CFT compound used to evaluate the

interplay between the nigrostriatal and digestive regions. Breaking through the technical limitations of the standard PET/CT with multi-beds scanning, the ultra-high sensitivity and 194-cm long axial field of view (AFOV) of the total-body PET/CT scanner enable us to simultaneously track the dynamic changes of the tracer distribution in the entire human body [21–23]. Meanwhile, parametric imaging offers additional quantitative values into varied pathophysiological alterations, and may also improve the visualization of pathophysiology, the precision of diagnosis, and the monitoring of disease progression [24].Incorporating with these tools may lead to a better understanding of the coordination between the brain function and other physiological activities [25].

Based on the novel technique of dynamic $[^{11}C]$CFT total-body PET/CT imaging, we aimed to employ the parametric imaging-based quantitative analysis using a simplified reference tissue model (SRTM) and the semi-quantitative measurement based on the standardized uptake value ratio (SUVR) to measure the dynamic total-body $[^{11}C]$CFT kinetics. The resulting parameters were then used to explore the potential correlations of estimates of the selected nigrostriatal and digestive regions by comparing PD patients and healthy volunteers.

Methods

Participants

Eleven participants including five untreated patients diagnosed as Parkinsons's disease (PD group) and six healthy volunteers as controls (HC group) respectively underwent $[^{11}C]$CFT total-body PET/CT scans in Department of Nuclear Medicine, Ren Ji Hospital from January to December 2021. The detailed clinical characteristics of all the participants were listed in Supplementary Table 1. Healthy volunteers were selected from health screening participants, based on the criteria of no notable history of major medical conditions or neuropsychiatric disorders, and no neoplastic diseases confirmed by $[^{18}F]$FDG PET/CT scans. This retrospective study followed the principles of the Declaration of Helsinki and has been approved by the ethics committee of Ren Ji Hospital with written informed consent waived.

Radiopharmaceutical preparation

The radionuclide, $^{11}CO_2$, was prepared by the medical cyclotron (HM-10, Sumitomo) in the Department of Nuclear Medicine, Ren Ji Hospital. $[^{11}C]$CFT was produced by an automatic synthesis module (CFN-MPS-200, Sumitomo)

according to the previously reported method [26]. The radiochemical purity of [11C]CFT was above 95%.

Dynamic total-body PET/CT acquisition and reconstruction

Each participant was subjected to a dynamic 75-min [11C]CFT PET scan on a total-body PET/CT scanner (uEXPLORER, United Imaging Healthcare) immediately after an intravenous bolus injection of 431.4 ± 75.6 MBq [11C]CFT from the lower limb, ensuring the participant's head within the scanner's high-sensitivity areas. The dynamic PET images were corrected for radioactive decay, scatter, attenuation and random, and were reconstructed into a matrix with a voxel size of $1.67 \times 1.67 \times 2.89$ mm^3 in x, y, z directions with ordered subset expectation maximization (OSEM) algorithm (4 iterations, and 20 subsets), incorporating time-of-flight (TOF) and point-spread function (PSF). The images were reconstructed into 97 frames (30×2 s, 12×5 s, 6×10 s, 4×30 s, 25×60 s, 15×120 s, 5×180 s) [27, 28].

Dynamic PET image processing

Volumes of interest (VOIs) were manually drawn within descending aorta, pancreas, stomach, and duodenum using PMOD 4.3 software (PMOD Technologies Ltd.). The frame-by-frame VOI delineation of stomach wall was performed based on the PET/CT fusion images with the minimal adjustment to each adjacent frame, avoiding the luminal content of the stomach. For the brain regions, all PET images were processed, firstly, by head motion correction based on the moving average reference method of Zhou et al. [24] using Statistical Parametric Mapping software (SPM12, Wellcome Department of Imaging Neuroscience) in the MATLAB (2019b, The MathWorks Inc.) environment, and secondly, by the spatial normalization of the PET images to the standard Montreal Neurologic Institute (MNI) space based on an MRI template [24]. The cerebral regions of caudate, putamen, pallidum, substantia nigra and occipital lobe were selected for the later analysis following the definition of brain VOI proposed by the Johns Hopkins Department of Radiology and then manually drawn on the MRI template in the standard MNI space [24]. Time activity curves (TACs) of all selected regions were then extracted. Based on the TACs, the mean standardized uptake value (SUV$_{mean}$) curves normalized by the ratio of the decay-corrected injected radiolabeled dose to body weight of the participant were generated. In the SUV$_{mean}$ curve analysis of the nigrostriatal nuclei, the separation time was defined as the time when the difference in group means between the SUV$_{mean}$ of HC and PD reached at least 10% of the mean SUV$_{mean}$ of the HC group.

Kinetic modeling

Using the SRTM with a linear regression and spatial constraint (LRSC) algorithm [29], the voxel-wise [11C]CFT kinetic analysis generated two parametric images: R$_1$ (the ratio of the transport rate constants of target to reference tissues) and DVR (distribution volume ratio of the target to reference tissues). The R$_1$ represents the relative transporter rate constant of tracer from vascular space to the target organs or brain regions, and DVR reflects the tracer specific binding to DAT. The occipital lobe region lacking DAT distribution was selected as the reference tissue. VOI-based SRTM fitting in PMOD 4.3 was implemented to examine the fit quality.

Additional blood input-based kinetic models were performed including the VOI-based two-tissue compartmental modeling (2T4K) [20], graphical analysis method of Logan plot [30], and bi-graphical analysis method using the relative equilibrium-based plot and the Gjedde-Patlak plot (RE-GP plots) [18] with the population-based metabolite-corrected TAC of descending aorta as the input [18], using PMOD 4.3 to estimate the tracer distribution independent from the selection of reference tissue. The total distribution volumes (V$_T$s) were estimated by 2T4K model fitting, Logan, and RE-GP plots.

SUVR calculation

SUVR, calculated as the ratio of the SUV of the target area to occipital lobe reference region, served as an approximation of early blood perfusion and DAT expression level. This method offered an advantage of a shorter scan acquisition time for clinical settings. The dynamic scanning period of [11C]CFT was subdivided into the early phase (SUVR$_{EP}$ for 1–3 min) and late phase (SUVR$_{LP}$ for 60–75 min), where SUVR$_{EP}$ was used to estimate R$_1$, and SUVR$_{LP}$ can be used as an approximation of the tracer specific binding to DAT resembling DVR [24].

Statistical analysis

All statistical analyses were performed using R (version 4.2.0) and GraphPad (version 9.0) software. Group estimates were represented by mean $\pm$ standard deviation (SD). Student's t test was performed to compare the mean of estimates between HC and PD groups. Pearson's correlation was employed to assess the agreement between the estimates generated by different approaches. Spearman's correlation analysis was used to compare the relationship between the target nigrostriatal and digestive regions. The $p < 0.05$ was considered statistically significant.

Results

Dynamic total-body [^{11}C]CFT PET Imaging

The schematic PET/CT acquisition protocol, representative total-body maximum intensity projection (MIP) images, and the transverse views of nigrostriatal and digestive regions acquired at different time points are presented in Fig. 1. During the dynamic total-body [^{11}C]CFT PET imaging up to 75 min, the tracer uptake was observed in both central and peripheral target regions across the body, including the deep brain regions such as the substantia nigra. Visual assessment revealed intact and persistent [^{11}C]CFT uptake in the nigrostriatal nuclei of HC, whereas PD patients displayed asymmetric DAT depletion in the corresponding areas. No distinct difference was observed from the visual assessment of digestive regions between the HC and PD groups.

Characterization of SUV$_{mean}$ curve

Figure 2A and B illustrate the SUV$_{mean}$ curves of descending aorta and occipital lobe in both HC and PD groups, demonstrating minimal variation in the curve patterns for these regions between the participant groups. Over time, the rising curves of the nigrostriatal regions began to diverge between the groups: the [^{11}C]CFT uptake in the HC group exhibited a continuous increase, whereas the PD group showed an earlier shift towards a state of "lesser uptake" (Fig. 2C; Table 1). In the putamen, an early separation in [^{11}C]CFT uptake curves was observed between the two groups (separation time = 2 min). The highest SUV$_{mean}$ values between the groups were also noted (8.59 ± 1.93 in HC vs. 5.09 ± 2.18 in PD, $p < 0.05$).

In both groups, the SUV$_{mean}$ curves of the pancreas and duodenum exhibited a "fast-in and slow-out" pattern,
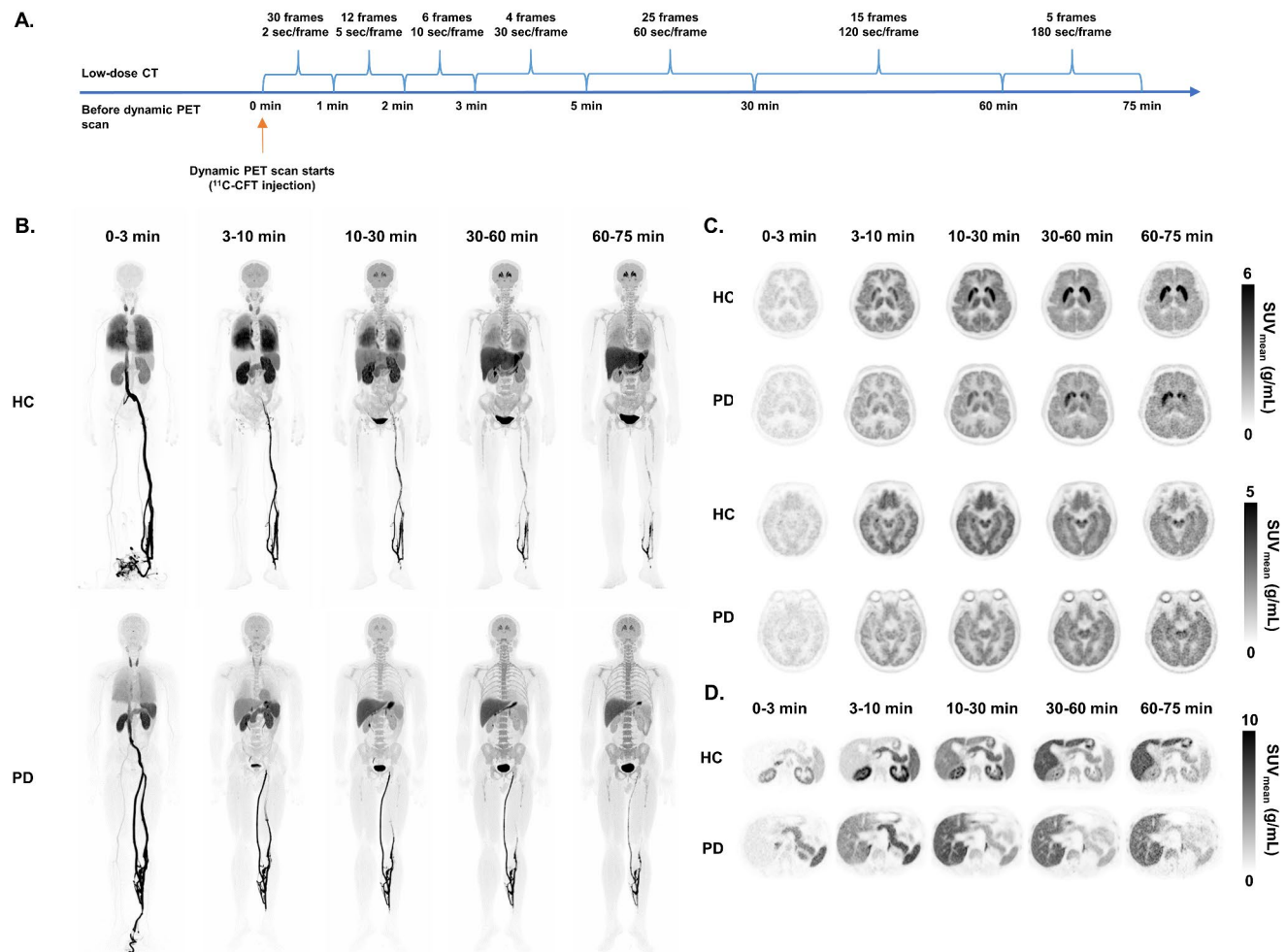
Fig. 1 **A** Total-body dynamic [^{11}C]CFT PET/CT scanning protocol (75 min, 97 frames). **B**–**D** Selected view from [^{11}C]CFT dynamic reconstructed images of a 53-year-old healthy volunteer (HC) and a 57-year-old Parkinson's disease patient (PD) at different timepoints. **B** Total-body maximum intensity projection (MIP) images. **C** Transverse views of cerebral nuclei both in the striatal and substantia nigra plane. The [^{11}C]CFT uptake in HC developed earlier and increased over time, while the nigrostriatal dopamine depletion was finally found in PD with a caudal-rostral gradient tendency, especially on the left side. **D** Transverse views of the upper abdomen. Abbreviation: HC, healthy controls; PD, Parkinson's disease patients
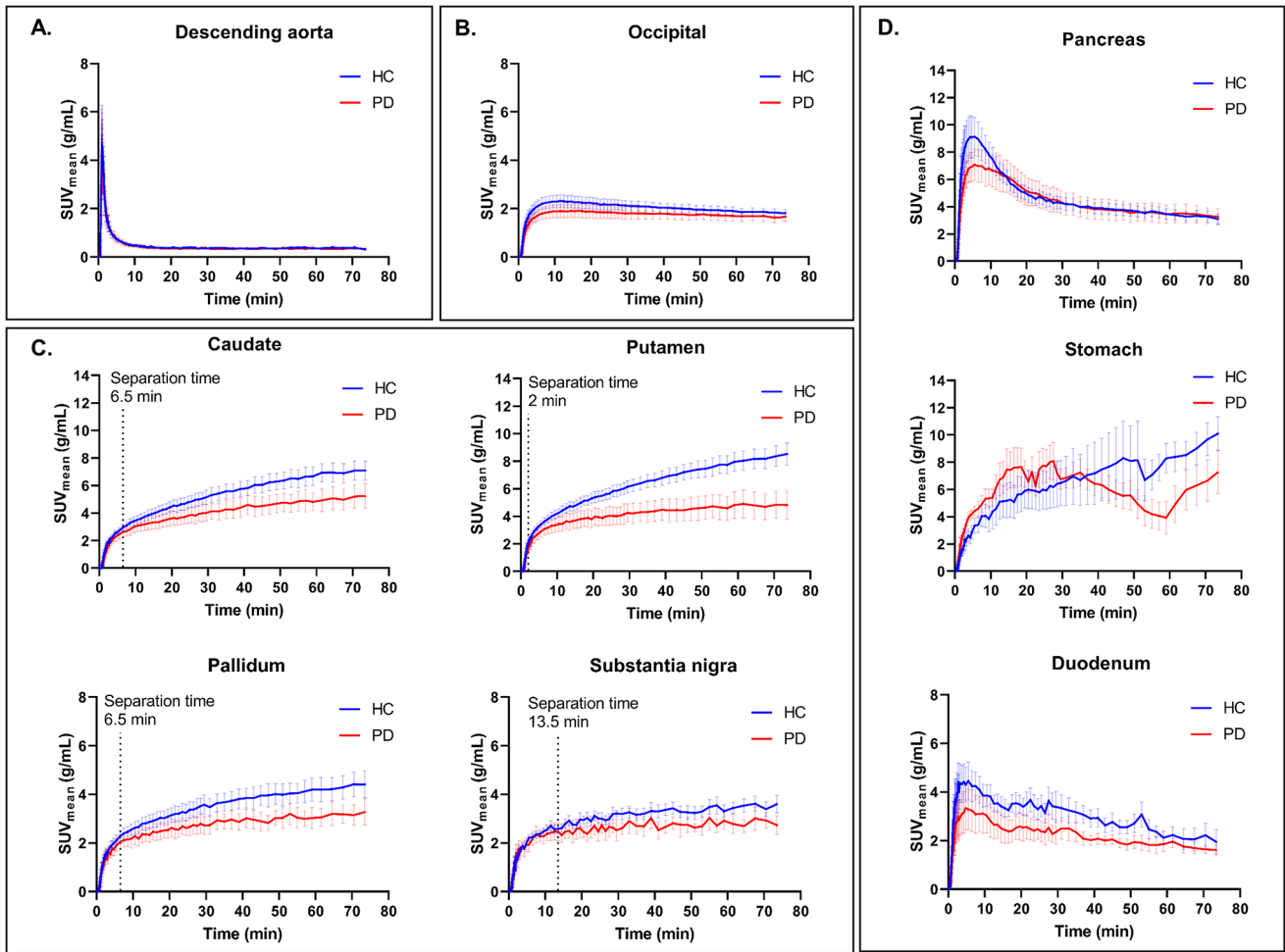
Fig. 2 Comparison of averaged SUV_{mean} curves in HC and PD group at the **A** descending aorta, **B** occipital lobe, selected **C** nigrostriatal nuclei regions and **D** digestive organs. Data are represented by mean ± standard error mean (SEM). Separation time between the averaged SUV_{mean} curves of HC and PD groups was marked on the curves for the nigrostriatal nuclei

Table 1 The SUV_{mean} curve characteristics of the target regions

| Uptake pattern	Organs	Separation time, min	Highest SUV_{mean}, mean ± SD, g/mL		
			HC	PD	p value
Gradually increasing	Caudate	6.5	7.16 ± 1.67	5.35 ± 1.93	0.13
	Putamen	2.0	8.59 ± 1.93	5.09 ± 2.18	0.02*
	Pallidum	6.5	4.49 ± 1.30	3.44 ± 1.10	0.19
	SN	13.5	3.88 ± 0.8	3.34 ± 0.93	0.32
Increasing with fluctuation	Stomach	N/A	11.80 ± 5.46	9.87 ± 2.66	0.49
Rapid increasing and slow decreasing	Duodenum	N/A	5.31 ± 1.89	3.84 ± 1.76	0.22
	Pancreas	N/A	9.62 ± 3.54	7.76 ± 2.38	0.35

Abbreviations SD, standard deviation; HC, healthy control; PD, Parkinson's disease patient; SN, substantia nigra

*$p < 0.05$

with the HC group showing higher peak activities in these organs than the PD group. For the stomach, a relatively quicker initial uptake in PD patients was observed, but the final SUV_{mean} in the HC group at 75 min appeared higher (Fig. 2D; Table 2).

R_1, DVR and SUVRs between HC and PD groups

The total-body [^{11}C]CFT PET parametric images based on the SRTM model were generated. The schematic representation of SRTM model and representative R_1 and DVR parametric images of HC and PD participants are illustrated in Fig. 3A and B, respectively. A statistically significant correlation was observed between the parameters of quantitative and semi-quantitative analysis, including R_1 and $SUVR_{EP}$ ($r = 0.78$, $p < 0.001$), DVR and $SUVR_{LP}$ ($r = 0.74$, $p < 0.001$) (Fig. 3C). In the comparison of the quantitative parameters between HC and PD groups, statistical significances were found between the HC and PD groups in terms
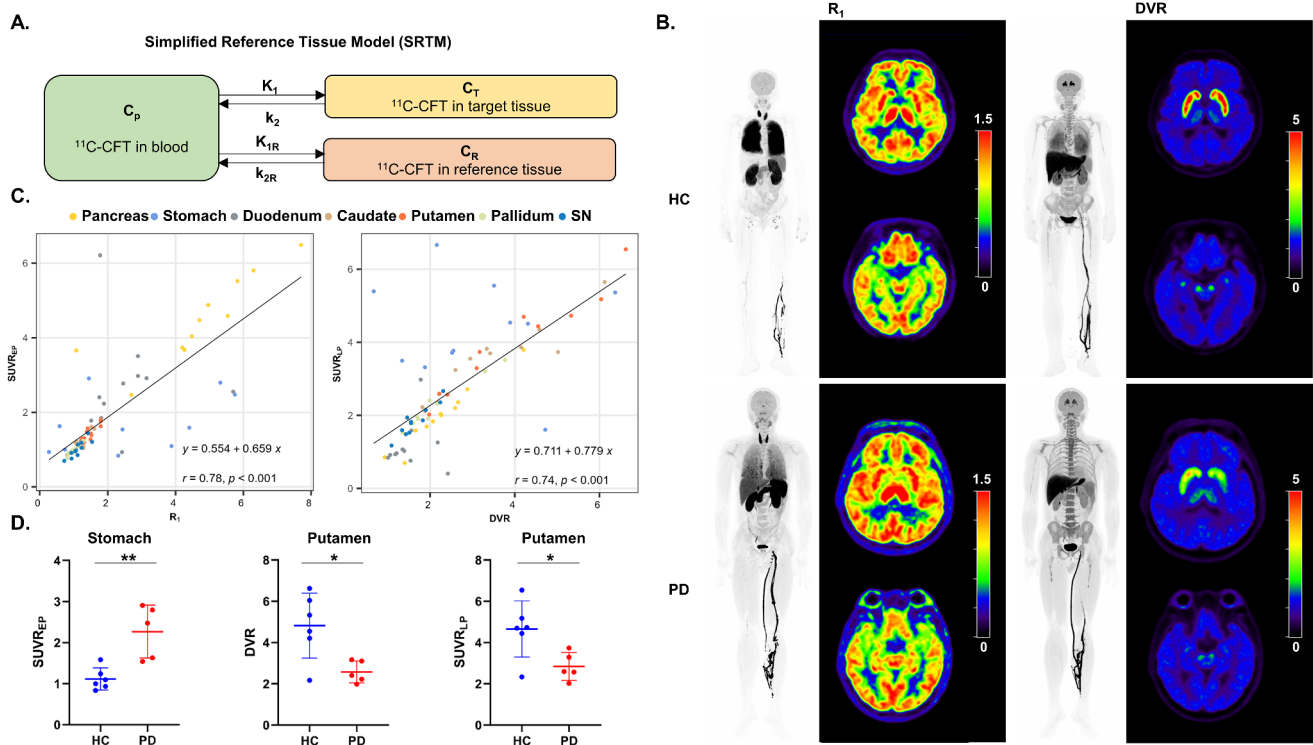
Fig. 3 **A** Schematic representation of the simplified reference tissue model (SRTM). **B** R_1 and DVR parametric images of HC and PD representatives. **C** Correlation between the SRTM estimates and semi-quantitative measurements. The semi-quantitative measurements for early perfusion (SUVR$_{EP}$) (left) and dopamine transporter density (SUVR$_{LP}$) (right) were both significantly correlated to the quantitative estimates (R_1 and DVR, respectively). **D** Significant differences between the HC and PD groups in SUVR$_{EP}$ of stomach (left) and both DVR (middle) and SUVR$_{LP}$ (right) of putamen. *, $p < 0.05$; **, $p < 0.01$. *Abbreviation* SN, substantia nigra

of SUVR$_{EP}$ of stomach (1.12 ± 0.27 vs. 2.27 ± 0.65 for HC and PD, $p < 0.01$) and both DVR and SUVR$_{LP}$ of putamen (DVR: 4.82 ± 1.58 vs. 2.58 ± 0.53, SUVR$_{LP}$: 4.65 ± 1.36 vs. 2.84 ± 0.67 for HC and PD, respectively, all $p < 0.05$) (Fig. 3D, Supplemental Table 2).

Correlation analyses to compare the DVR estimated from SRTM with the distribution volume (V_T) from 2T4K, Logan and RE-GP plots are presented in Supplemental Fig. 1. The V_T showed significant Pearson's correlation with DVR estimates from SRTM (2T4K: $r = 0.94$; Logan plot: $r = 0.88$; RE-GP plot, $r = 0.85$; all $p < 0.001$).

Correlations among the target nigrostriatal and digestive regions

Figure 4A and B demonstrate that a negative correlation pattern existed between the stomach and substantia nigra for early perfusion estimates of R_1 and SUVR$_{EP}$ in the HC group ($r = -0.83$, $p < 0.05$ for R_1, and $r = -0.94$, $p < 0.01$ for SUVR$_{EP}$, respectively), whereas this correlation was not statistically significant in the PD group ($r = -0.70$, $p = 0.19$ for R_1; $r = 0.50$, $p = 0.39$ for SUVR$_{EP}$). Figure 4C and D illustrate statistically significant positive correlations between pancreas and putamen for tracer density estimates DVR

and SUVR$_{LP}$ in the HC group ($r = 0.94$, $p < 0.01$ for DVR; $r = 1.00$, $p < 0.001$ for SUVR$_{LP}$), but these correlation coefficients were notably lower in the PD group ($r = 0.60$, $p = 0.29$ for DVR; $r = 0.30$, $p = 0.62$ for SUVR$_{LP}$, respectively). We also examined the correlation between V_T of pancreas and putamen estimated from the VOI-based 2T4K ($r = 0.77$, $p = 0.10$ for HC, $r = 0.10$, $p = 0.95$ for PD), Logan plot ($r = 1.00$, $p < 0.01$ for HC, $r = -0.30$, $p = 0.68$ for PD), and RE-GP plot ($r = 0.94$, $p < 0.05$ for HC, $r = -0.30$, $p = 0.68$ for PD). The results from plasma input-based kinetic modeling demonstrated similar linear correlation pattern in HC rather than PD group (Supplemental Fig. 2).

Figure 5 shows the correlations for all target nigrostriatal and digestive regions in both HC and PD groups in terms of the kinetic and semi-quantitative estimates, with detailed scatter plots presented in Supplemental Fig. 3. Significant positive correlations for DVR were noted across all four nigrostriatal nuclei ($r = 0.94$ to 1.00, all $p < 0.05$) within the HC group, while these correlations were considerably diminished in the PD group. In the HC group, the DVR of the pancreas also showed significant correlations with the other three nigrostriatal nuclei, namely, caudate, pallidum, and substantia nigra ($r = 0.83$, $p < 0.05$ for all). In contrast, no significant correlations were observed between
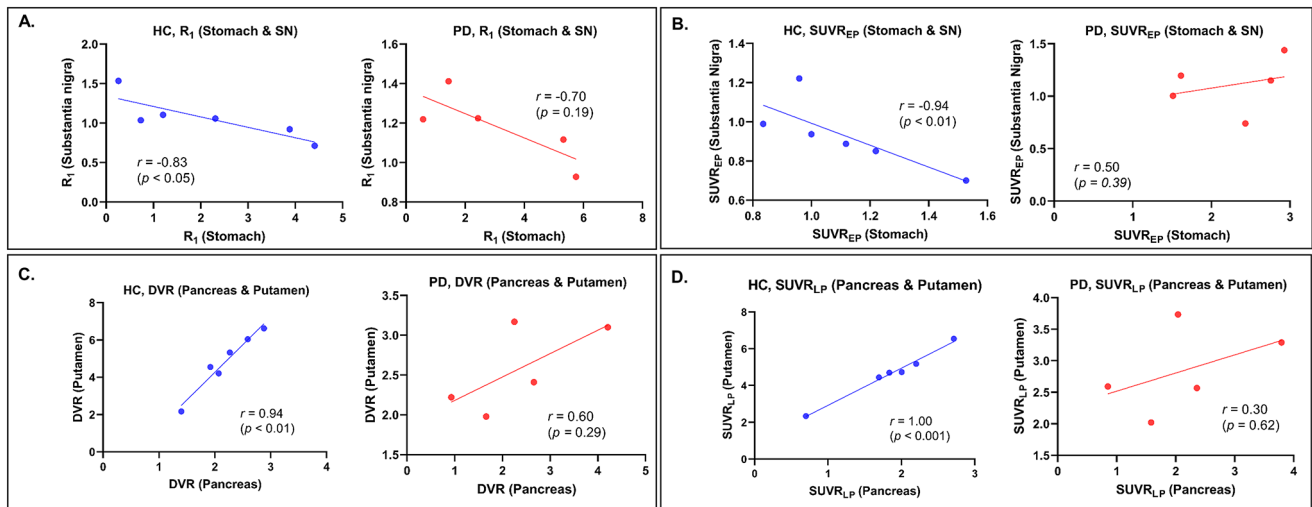
Fig. 4 Scatter plots of the Spearman's rank correlation analyses between stomach and substantia nigra in terms of **A** R_1 and **B** $SUVR_{EP}$, and between pancreas and putamen in terms of **C** DVR and **D** $SUVR_{LP}$, for both HC and PD groups. *Abbreviation* SN, substantia nigra

the pancreas and any other nigrostriatal regions in the PD group.

Discussion

Acknowledging the diverse and systemic symptoms in PD, our study aims to propose a novel paradigm that surpasses traditional brain-focused research by leveraging [11C]CFT, a tracer targeting DAT, and integrated dynamic total-body PET/CT imaging. This image-based approach is designed to comprehensively assess alterations and interactions between the nigrostriatal and digestive regions. Dopamine serves as a protective agent for human digestive system, preventing gastric and intestinal mucosa from injury, resisting against peptic ulcer, and promoting ulcer healing [31]. PD patients also have a relatively high incidence of duodenal ulcers, while gastrointestinal dysfunction or dysmotility are often likely due to DA deficiency or peripheral DAT depletion [32]. Most of the previous reports on DA and DAT have focused on their neurotransmitter function only in the central nerve system (CNS). However, certain peripheral organs also have abundant DAT expressions. Recent studies have indicated that at the time when pathological α-synuclein aggregation was found in the submucosal and myenteric neurons, there also existed abnormal changes of dopaminergic neurons in these enteric plexuses in both PD patients and animal models [33–35]. A potential relationship between peripheral and central DAT may assess the disease progression and the effectiveness of pharmacotherapies in PD [36]. Therefore, it is necessary to employ a macroscopic approach for integrated evaluation of the DA homeostasis in both the CNS and ENS.

The quantitative method incorporated with kinetic modeling provides direct information on the specific biologic process, representing the relative transporter rate constant and tissue density of DAT, whereas the semi-quantitative method of SUVR facilitates shorter scan acquisition and thus is often favored in clinical settings to estimate such parameters [24]. The statistically significant difference between HC and PD groups in terms of putamen DVR and $SUVR_{LP}$ was in accordance with the previous human striatal [11C]CFT studies [15, 17]. The correlation between DVR and $SUVR_{LP}$ also indicated a good agreement between the quantitative and semi-quantitative measurements in putamen. However, in all the regions examined, the correlation between DVR and $SUVR_{LP}$ in the stomach appeared to deviate from a linear fit. Acquiring the continuous TACs for stomach has been a challenge for previous studies on the dynamic PET studies of peripheral organs due to the peristalsis and its adjacency to the pancreas and liver [37], which may contributed to the discrepancies between the quantitative and SUVR values, as well as the fluctuation in stomach TACs. The frame-by-frame VOI delineation of the stomach wall avoiding the luminal content based on the PET/CT fusion used in this study was expected to reduce the motion effect of peristalsis. More sophisticated approaches of motion correction in the future are desired to further reduce the bias caused by peristalsis in dynamic gastral PET quantification.

Both the voxel-based SRTM modeling and SUVR analysis in this study suggested that, for the healthy population, there was a negative correlation of the relative blood perfusion estimates R_1 and $SUVR_{EP}$ between the stomach and substantia nigra. In terms of the DAT density estimates DVR and $SUVR_{LP}$, the positive correlation between pancreas and putamen was also observed. The preliminary results from previous study identified statistically significant Spearman's

Fig. 5 Spearman's rank correlation between all nigrostriatal nuclei and digestive organs based on the quantitative estimates of **A** R_1 and **B** DVR, and semi-quantitative measurements of **C** $SUVR_{EP}$ and **D** $SUVR_{LP}$ in HC and PD groups. The upper triangle gives the graphical demonstration of the correlation, where the orientations of the ellipses represent the signs of the correlation coefficient (upper-left to lower-right, negative; lower-left to upper-right, positive), and colors and width represent the magnitude of the coefficients. The asterisks represent the significance (*, $p < 0.05$; **, $p < 0.01$; ***, $p < 0.001$). The lower triangle displays the correlation coefficient r. *Abbreviation* SN, substantia nigra
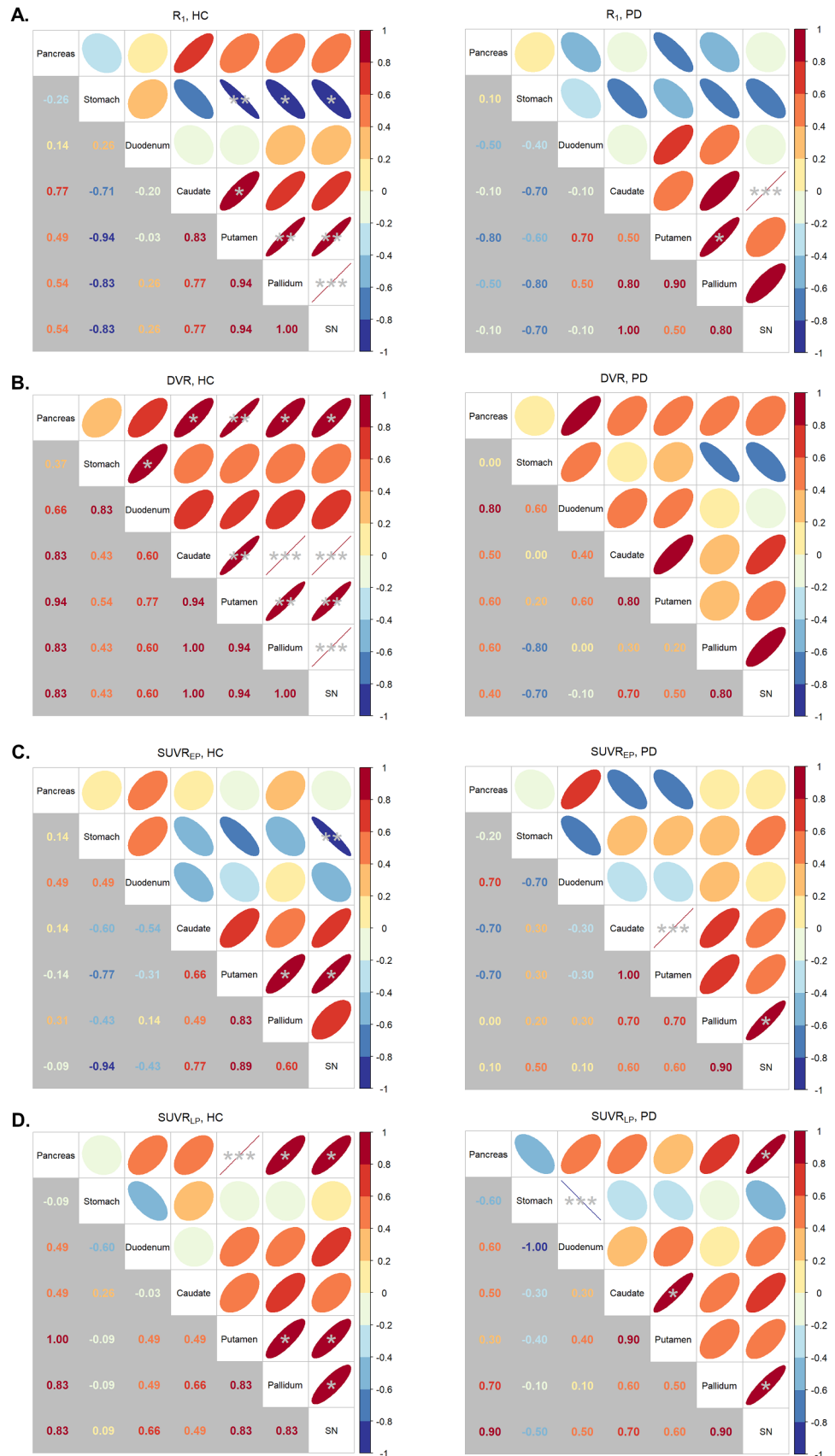
correlation between the late-phase SUV_{mean} of pancreas and putamen in the healthy participants rather than PD patients based on dynamic total-body [^{11}C]CFT PET/CT imaging [38], which was in accordance to the DVR and $SUVR_{LP}$ correlation results of pancreas and putamen in this study. Buttarelli et al. demonstrated a lack of correlation between the densitometric measurements of DAT immunoreactivity in peripheral blood lymphocytes and the DAT binding in the striatal regions obtained by [^{123}I]fluopane SPECT imaging in PD patients [39], suggesting the loss of correlation between central and peripheral DAT in PD patients. Garrido-Gil et al. also reported early changes in the nigrostriatal dopaminergic homeostasis and dopaminergic neuron death in PD rat models [40]. A possible hypothesis may be that the potential intrinsic correlation upon the nigrostriatal and digestive axis in healthy individuals might be disrupted by the occurrence of PD. Nevertheless, it is important to note that this study's scope is limited, being a small-scale analysis involving only six HC individuals and five PD patients. Therefore, these preliminary findings should be interpreted with caution. Future studies recruiting larger cohorts are expected to confirm the results.

Despite the uEXPLORER's high sensitivity allowing for imaging at later time points after the administration of the radiotracer [21], challenges in patient recruitment and prolonged scans beyond 75 min were encountered due to PD patients' intolerance for long scans and the absence of suitable total-body PET motion correction algorithms tailored for extended duration. Previous studies recommended a 90-min dynamic scanning period for [^{11}C]CFT quantification in brain [17, 18, 20]. Thus, considering the slow kinetics of [^{11}C]CFT and the continuously increasing TACs of caudate and putamen in the HC group at 75 min, we additionally performed computer simulation to investigate whether the striatal DVR estimates from SRTM using 75 min of data are comparable to that with 90-min data for both HC and PD participants (Supplemental Tables 3 and Supplemental Fig. 4). The Pearson's correlation analysis revealed a statistically significant relationship ($r = 0.99$, $p < 0.001$) between the DVR values obtained from 75- and 90-min data under low tissue noise conditions and a noise-free reference tissue. The largest difference in the averaged percent bias for the DVR estimates, derived from 75- and 90-min data across all noise levels, was under 10%. The visual inspection of fit quality and percent standard error of estimates in the nigrostriatal regions of a representative HC participant and PD patient presented in Supplemental Fig. 5 also demonstrated acceptable fit quality of SRTM with true 75-min striatal data. The results suggested that the striatal DVRs estimated from SRTM using 75 min of dynamic data are comparable to those derived from 90 min of data.

The SRTM with LRSC parametric imaging algorithm demonstrated a higher computational efficiency and voxel-level stability compared to that of nonlinear least squares method in describing the kinetics of [^{11}C]CFT in rats presented by Gunn et al. [41] and Zhou et al. [29]. Other advantages of the SRTM method include the avoidance of arterial cannulation and metabolite measurements [42]. However, the assumption of constant non-displaceable binding levels in both target and reference tissues in SRTM [29, 41] might not apply to the context of total-body quantification with diverse non-specific bindings across various target organs. To our understanding, no existing research has thoroughly addressed the choice of reference for kinetic measurements in dynamic total-body [^{11}C]CFT PET quantification. Using a single reference for both the nigrostriatal and digestive regions serves as a preliminary attempt at total-body PET quantification with a reversibly binding brain tracer. We chose the DVR over the binding potential (BP_{ND}) as a surrogate for DAT density, where DVR serves as a normalization reflecting the ratio of distribution volume of the target to reference tissue [29, 43]. We additionally implemented the model selection of reference-independent VOI-wise blood input-based kinetic modeling, and indicated that the 2T4K, Logan and RE-GP plots were the suitable blood input-based model for total-body [^{11}C]CFT quantification (Supplemental Tables 4–5, Supplemental Fig. 6). The significant Pearson's correlation between the DVR estimated from SRTM and the V_T derived from 2T4K, Logan and RE-GP plots then also suggested reliable total-body DVR estimates by SRTM using occipital lobe as the reference. The presence of a similar correlation pattern in the blood input-based V_T between the pancreas and putamen in HC but not in PD group suggests that the choice of reference may have minimal impact on the observed differences in correlation patterns within this study. Future research are advised to advance quantification methods that validate model and reference choices for both nigrostriatal and digestive organs, aiming to mitigate potential biases arising from variations in non-specific tissue bindings.

[^{11}C]CFT PET was proven as a suitable tracer to reflect the striatal DAT level in humans for its high target-to-non-target ratio [17, 18, 20]. Though [^{3}H]CFT has been shown to have some affinity to other monoamine transporters such as serotonin transporters (SERT) and norepinephrine transporters (NET) in animal studies [44, 45], Forsback et al. [19] found that after GBR12909 (a selective DAT antagonist) treatment, DAT-specific binding in the pancreas of the rats showed a significant declining trend, whereas no specific binding of ^{18}F activity of SERT and NET was found in the periphery, suggesting the selectivity of [^{18}F]CFT to DAT in the peripheral organs. A pharmacological blockade study with human participants receiving selective DAT antagonist

could be used in the future to confirm the specific binding especially in human digestive organs.

Metabolites of [11C]CFT may play a significant role in the quantification, especially in the digestive organs with the lack of blood-brain barrier. Our study is limited by not identifying a specific fraction of the intact [11C]CFT signal for the digestive regions in human. Nevertheless, previous studies suggested that [11C]WIN 35,428 (β-CFT), as a phenyltropane compound with the absence of one of the ester groups of cocaine [46, 47], may be more resistant to the metabolic degradation [20]. Laakso et al. stated that the metabolized activity of [18F]CFT would be under 20–30% at 3–4 h post-injection, and whether the metabolites cross the blood-brain barrier was not known [48]. We also employed the population-based metabolite correction on the image-derived input function using the population data from Zhou et al. [18] in the blood input-based kinetic modeling of this study. The plasma parent fraction using the population data of 19 normal human participants [18] as shown in Supplemental Fig. 7 demonstrated that more than 85% of the intact [11C]CFT remained in the plasma at 75 min. In addition, we assessed the 2T4K V_T for all target areas using VOI-based analysis, employing the image-derived descending aorta TAC as input, both with and without applying population-based metabolite correction, as demonstrated in Supplemental Fig. 8. The comparison revealed a significant correlation ($r = 0.99$, $p < 0.001$) between the V_T estimated by two methods. The absence of metabolite correction induced an average of 7.2% underestimation of V_T. Our results suggested that the tracer metabolism of [11C]CFT was not expected to dramatically change the tracer distribution in the nigrostriatal and digestive regions. The previous literature also showed that the liver is able to clear the circulating catecholamines, including DA [7]. The liver SUV_{mean} curves of HC and PD in our study suggested a slightly higher SUV_{mean} at 75 min in the PD group but no significant difference across two groups (student's t test, 7.21 ± 0.95 for HC vs. 7.85 ± 2.83 for PD, $p = 0.65$) (Supplemental Fig. 9A). This result suggests that there may be a negligible difference in peripheral metabolites of DA levels between HC and PD groups after the physiological control by the liver, which should be validated in a larger cohort.

Although an age-dependent decrease in the striatal uptake of [11C]CFT was observed in rats by Kawamura et al. [49], the kinetic analysis-based striatal binding potential of [11C]CFT was not identified in the same study. In a human L-6- [18F]fluoro-Dopa PET study, no decline was found in tracer uptake of the volunteers with age 27–76 [50]. With our limited sample size, we were unable to identify a clear relationship between age and [11C]CFT kinetic estimates of target regions. Recruiting more participants of older age in the HC group and implementing relevant quantification methods might aid in quantifying the age-dependent effects.

We also noted high tracer uptake at late phase in the lungs of three HC participants and one PD patient (Supplemental Fig. 10). The lung SUV_{mean} curves demonstrated that the peak SUV_{mean} of the HC was higher than that in the PD group (Supplemental Fig. 9B), yet the difference was not statistically significant (student's t test, 6.27 ± 2.44 for HC vs. 4.99 ± 2.27 for PD, $p = 0.40$). No history of lung-related diseases was identified in any of the eleven participants from the medical record or CT images. A prior investigation into DAT immunoreactivity indicated high DAT expression in the lungs [7], hinting at a potential avenue for future research exploration.

The motion and partial volume correction for small tissue in total-body PET quantification are still challenging. The accuracy of the estimated model parameters might be biased by body motion or partial volume effects on our dynamic PET data, as fully recognized and discussed in a previous dynamic total-body PET study [28, 51]. The moving average reference-based head motion correction and frame-by-frame VOI delineation of the stomach wall performed in this study were expected to reduce such bias. We also employed the OSEM with PSF in our image reconstruction to reduce the partial volume effects for both HC and PD groups. The blood pool we chose for the input function of the compartment modeling was descending aorta, which demonstrated negligible motion during dynamic scans for its proximity to the spine. Previous study also showed the feasibility of using descending aorta as the input function to generate high-quality parametric images in the dynamic total-body study of [18F]FDG [51]. More appropriate motion and partial volume correction algorithms designated for dynamic total-body PET/CT quantification could be applied to further reduce the artifacts.

Conclusion

The R_1 and DVR parametric images generated from the SRTM model with LRSC algorithm, along with the semi-quantitative measurements of $SUVR_{EP}$ and $SUVR_{LP}$, were proposed to quantify the dynamic total-body [11C]CFT PET/CT in HC and PD groups. The distinct patterns in correlative interplays between the nigrostriatal and digestive regions of HC and PD participants may offer new perspectives in comprehending the disease mechanism.

Declarations

Conflict of interest All authors declare that they have no conflict of interest.

References

1. Kalia LV, Lang AE. Parkinson's disease. Lancet. 2015;386:896–912. https://doi.org/10.1016/s0140-6736(14)61393-3.
2. Horsager J, Andersen KB, Knudsen K, Skjaerbaek C, Fedorova TD, Okkels N, et al. Brain-first versus body-first Parkinson's disease: a multimodal imaging case-control study. Brain. 2020;143:3077–88. https://doi.org/10.1093/brain/awaa238.
3. Adamantidis A. How the gut talks to the brain. Science. 2022;376:248–9. https://doi.org/10.1126/science.abo7933.
4. Tóth BE, Vecsernyés M, Zelles T, Kádár K, Nagy GM. Role of peripheral and brain-derived dopamine (DA) in immune regulation. Adv Neuroimmune Biology. 2012;3:111–55. https://doi.org/10.3233/nib-2012-012044.
5. Li ZS, Pham TD, Tamir H, Chen JJ, Gershon MD. Enteric dopaminergic neurons: definition, Developmental Lineage, and effects of extrinsic denervation. J Neurosci. 2004;24:1330–9. https://doi.org/10.1523/jneurosci.3982-03.2004.
6. Mitsuma T, Rhue H, Hirooka Y, Kayama M, Wago T, Takagi J, et al. Distribution of dopamine transporter in the rat: an immunohistochemical study. Endocr Regul. 1998;32:71–5.
7. Eisenhofer G. The role of neuronal and extraneuronal plasma membrane transporters in the inactivation of peripheral catecholamines. Pharmacol Ther. 2001;91:35–62. https://doi.org/10.1016/s0163-7258(01)00144-9.
8. Tian YM, Chen X, Luo DZ, Zhang XH, Xue H, Zheng LF, et al. Alteration of dopaminergic markers in gastrointestinal tract of different rodent models of Parkinson's disease. Neuroscience. 2008;153:634–44. https://doi.org/10.1016/j.neuroscience.2008.02.033.
9. Ustione A, Piston DW. Dopamine synthesis and D3 receptor activation in pancreatic beta-cells regulates insulin secretion and intracellular [Ca(2+)] oscillations. Mol Endocrinol. 2012;26:1928–40. https://doi.org/10.1210/me.2012-1226.
10. Cerantola S, Caputi V, Contarini G, Mereu M, Bertazzo A, Bosi A, et al. Dopamine transporter genetic reduction induces Morpho-Functional changes in the enteric nervous system. Biomedicines. 2021;9. https://doi.org/10.3390/biomedicines9050465.
11. Walker JK, Gainetdinov RR, Mangel AW, Caron MG, Shetzline MA. Mice lacking the dopamine transporter display altered regulation of distal colonic motility. Am J Physiol Gastrointest Liver Physiol. 2000;279:G311–8. https://doi.org/10.1152/ajpgi.2000.279.2.G311.
12. Hamamah S, Aghazarian A, Nazaryan A, Hajnal A, Covasa M. Role of Microbiota-Gut-Brain Axis in regulating Dopaminergic Signaling. Biomedicines. 2022;10. https://doi.org/10.3390/biomedicines10020436.
13. Hartstra AV, Schuppel V, Imangaliyev S, Schrantee A, Prodan A, Collard D, et al. Infusion of donor feces affects the gut-brain axis in humans with metabolic syndrome. Mol Metabolism. 2020;42:101076. https://doi.org/10.1016/j.molmet.2020.101076.
14. Zhu S, Ju Z, Wu P, Liu F, Ge J, Zhang H, et al. The Parkinson's disease progression neuroimaging initiative. Behav Neurol. 2021;2021:2230196. https://doi.org/10.1155/2021/2230196.
15. Sun X, Liu F, Liu Q, Gai Y, Ruan W, Wimalarathne DN, et al. Quantitative research of (11)C-CFT and (18)F-FDG PET in Parkinson's Disease: a Pilot Study with NeuroQ Software. Front Neurosci. 2019;13:299. https://doi.org/10.3389/fnins.2019.00299.
16. Liu FT, Ge JJ, Wu JJ, Wu P, Ma Y, Zuo CT, et al. Clinical, dopaminergic, and metabolic correlations in Parkinson Disease: a dual-Tracer PET Study. Clin Nucl Med. 2018;43:562–71. https://doi.org/10.1097/RLU.0000000000002148.
17. Ouchi Y, Yoshikawa E, Okada H, Futatsubashi M, Sekine Y, Iyo M, et al. Alterations in binding site density of dopamine transporter in the striatum, orbitofrontal cortex, and amygdala in early Parkinson's disease: compartment analysis for beta-CFT binding with positron emission tomography. Ann Neurol. 1999;45:601–10.
18. Zhou Y, Ye W, Brasic JR, Wong DF. Multi-graphical analysis of dynamic PET. NeuroImage. 2010;49:2947–57. https://doi.org/10.1016/j.neuroimage.2009.11.028.
19. Forsback S, Marjamaki P, Eskola O, Bergman J, Rokka J, Gronroos T, et al. [18F]CFT synthesis and binding to monoamine transporters in rats. EJNMMI Res. 2012;2:3. https://doi.org/10.1186/2191-219X-2-3.
20. Wong DF, Yung B, Dannals RF, Shaya EK, Ravert HT, Chen CA, et al. In vivo imaging of baboon and human dopamine transporters by positron emission tomography using [11 C]WIN 35,428. Synapse. 1993;15:130–42. https://doi.org/10.1002/syn.890150205.
21. Badawi RD, Shi H, Hu P, Chen S, Xu T, Price PM, et al. First human imaging studies with the EXPLORER Total-Body PET scanner. J Nucl Med. 2019;60:299–303. https://doi.org/10.2967/jnumed.119.226498.
22. Spencer BA, Berg E, Schmall JP, Omidvari N, Leung EK, Abdelhafez YG, et al. Performance evaluation of the uEXPLORER Total-Body PET/CT scanner based on NEMA NU 2-2018 with additional tests to characterize PET scanners with a long Axial Field of View. Journal of nuclear medicine: official publication. Soc Nuclear Med. 2021;62:861–70. https://doi.org/10.2967/jnumed.120.250597.
23. Zhang X, Cherry SR, Xie Z, Shi H, Badawi RD, Qi J. Subsecond total-body imaging using ultrasensitive positron emission tomography. Proc Natl Acad Sci USA. 2020;117:2265–7. https://doi.org/10.1073/pnas.1917379117.
24. Zhou Y, Flores S, Mansor S, Hornbeck RC, Tu Z, Perlmutter JS, et al. Spatially constrained kinetic modeling with dual reference tissues improves (18)F-flortaucipir PET in studies of Alzheimer disease. Eur J Nucl Med Mol Imaging. 2021;48:3172–86. https://doi.org/10.1007/s00259-020-05134-w.
25. Nardo L, Schmall JP, Werner TJ, Malogolowkin M, Badawi RD, Alavi A. Potential roles of total-body PET/Computed tomography in Pediatric Imaging. PET Clin. 2020;15:271–9. https://doi.org/10.1016/j.cpet.2020.03.009.
26. Tang G, Tang X, Deng H, Wang H, Wen F, Yi C, et al. Efficient preparation of [11 C]CH3Br for the labeling of [11 C]CH3-containing tracers in positron emission tomography clinical practice. Nucl Med Commun. 2011;32:466–74. https://doi.org/10.1097/MNM.0b013e3283438f9a.
27. Chen R, Yang X, Ng YL, Yu X, Huo Y, Xiao X, et al. First total-body kinetic modeling and parametric imaging of dynamic (68) Ga-FAPI-04 PET in pancreatic and gastric cancer. J Nuclear

Medicine: Official Publication Soc Nuclear Med. 2023. https://doi.org/10.2967/jnumed.122.264988.

28. Chen R, Yang X, Yu X, Zhou X, Ng YL, Zhao H, et al. Tumor-to-blood ratio for assessment of fibroblast activation protein receptor density in pancreatic cancer using [(68)Ga]Ga-FAPI-04. Eur J Nucl Med Mol Imaging. 2022. https://doi.org/10.1007/s00259-022-06010-5.

29. Zhou Y, Endres CJ, Brasic JR, Huang SC, Wong DF. Linear regression with spatial constraint to generate parametric images of ligand-receptor dynamic PET studies with a simplified reference tissue model. NeuroImage. 2003;18:975–89. https://doi.org/10.1016/s1053-8119(03)00017-x.

30. Logan J, Fowler JS, Volkow ND, Wolf AP, Dewey SL, Schlyer DJ, et al. Graphical analysis of reversible radioligand binding from time-activity measurements applied to [N-11 C-methyl]-(-)-cocaine PET studies in human subjects. J Cereb Blood flow Metabolism: Official J Int Soc Cereb Blood Flow Metabolism. 1990;10:740–7. https://doi.org/10.1038/jcbfm.1990.127.

31. Mezey E, Eisenhofer G, Harta G, Hansson S, Gould L, Hunyady B, et al. A novel nonneuronal catecholaminergic system: exocrine pancreas synthesizes and releases dopamine. Proc Natl Acad Sci USA. 1996;93:10377–82. https://doi.org/10.1073/pnas.93.19.10377.

32. Mezey E, Eisenhofer G, Hansson S, Hunyady B, Hoffman BJ. Dopamine produced by the stomach may act as a paracrine/autocrine hormone in the rat. Neuroendocrinology. 1998;67:336–48. https://doi.org/10.1159/000054332.

33. Singaram C, Ashraf W, Gaumnitz EA, Torbey C, Sengupta A, Pfeiffer R, et al. Dopaminergic defect of enteric nervous system in Parkinson's disease patients with chronic constipation. Lancet. 1995;346:861–4. https://doi.org/10.1016/s0140-6736(95)92707-7.

34. Anderson G, Noorian AR, Taylor G, Anitha M, Bernhard D, Srinivasan S, et al. Loss of enteric dopaminergic neurons and associated changes in colon motility in an MPTP mouse model of Parkinson's disease. Exp Neurol. 2007;207:4–12. https://doi.org/10.1016/j.expneurol.2007.05.010.

35. Li X, Yang W, Li X, Chen M, Liu C, Li J, et al. Alpha-synuclein oligomerization and dopaminergic degeneration occur synchronously in the brain and colon of MPTP-intoxicated parkinsonian monkeys. Neurosci Lett. 2020;716:134640. https://doi.org/10.1016/j.neulet.2019.134640.

36. Mackie P, Lebowitz J, Saadatpour L, Nickoloff E, Gaskill P, Khoshbouei H. The dopamine transporter: an unrecognized nexus for dysfunctional peripheral immunity and signaling in Parkinson's Disease. Brain Behav Immun. 2018;70:21–35. https://doi.org/10.1016/j.bbi.2018.03.020.

37. Gjerloff T, Fedorova T, Knudsen K, Munk OL, Nahimi A, Jacobsen S, et al. Imaging acetylcholinesterase density in peripheral organs in Parkinson's disease with 11 C-donepezil PET. Brain. 2015;138:653–63. https://doi.org/10.1093/brain/awu369.

38. Xin M, Li L, Wang C, Wang Y, Gu Y, Zhang C, et al. An investigation of the brain-GI relationships in Parkinson's disease by imaging dopamine transporter in dynamic 11 C-CFT total-body PET/CT. J Nucl Med. 2022;63:2480.

39. Buttarelli FR, Capriotti G, Pellicano C, Prosperi D, Circella A, Festa A, et al. Central and peripheral dopamine transporter reduction in Parkinson's disease. Neurol Res. 2009;31:687–91. https://doi.org/10.1179/174313209X383259.

40. Garrido-Gil P, Rodriguez-Perez AI, Dominguez-Meijide A, Guerra MJ, Labandeira-Garcia JL. Bidirectional neural Interaction between Central Dopaminergic and Gut lesions in Parkinson's Disease models. Mol Neurobiol. 2018;55:7297–316. https://doi.org/10.1007/s12035-018-0937-8.

41. Gunn RN, Lammertsma AA, Hume SP, Cunningham VJ. Parametric imaging of ligand-receptor binding in PET using a simplified reference region model. NeuroImage. 1997;6:279–87. https://doi.org/10.1006/nimg.1997.0303.

42. Lammertsma AA, Hume SP. Simplified reference tissue model for PET receptor studies. NeuroImage. 1996;4:153–8. https://doi.org/10.1006/nimg.1996.0066.

43. Zhou Y, Resnick SM, Ye W, Fan H, Holt DP, Klunk WE, et al. Using a reference tissue model with spatial constraint to quantify [11 C]Pittsburgh compound B PET for early diagnosis of Alzheimer's disease. NeuroImage. 2007;36:298–312. https://doi.org/10.1016/j.neuroimage.2007.03.004.

44. Kaufman MJ, Madras BK. [3H]CFT ([3H]WIN 35,428) accumulation in dopamine regions of monkey brain: comparison of a mature and an aged monkey. Brain Res. 1993;611:322–5. https://doi.org/10.1016/0006-8993(93)90519-s.

45. Aloyo VJ, Pazdalski PS, Kirifides AL, Harvey JA. Behavioral sensitization, behavioral tolerance, and increased [3H]WIN 35,428 binding in rabbit caudate nucleus after repeated injections of cocaine. Pharmacology, biochemistry, and behavior. 1995;52:335–40. https://doi.org/10.1016/0091-3057(95)00101-2.

46. Clarke RL, Daum SJ, Gambino AJ, Aceto MD, Pearl J, Levitt M, et al. Compounds affecting the central nervous system. 4. 3 Beta-phenyltropane-2-carboxylic esters and analogs. J Med Chem. 1973;16:1260–7. https://doi.org/10.1021/jm00269a600.

47. Carroll FI, Lewin AH, Boja JW, Kuhar MJ. Cocaine receptor: biochemical characterization and structure-activity relationships of cocaine analogues at the dopamine transporter. J Med Chem. 1992;35:969–81. https://doi.org/10.1021/jm00084a001.

48. Laakso A, Bergman J, Haaparanta M, Vilkman H, Solin O, Hietala J. [18F]CFT [(18F)WIN 35,428], a radioligand to study the dopamine transporter with PET: characterization in human subjects. Synapse. 1998;28:244–50. https://doi.org/10.1002/(SICI)1098-2396(199803)28:3<244::AID-SYN7>3.0.CO;2-A.

49. Kawamura K, Oda K, Ishiwata K. Age-related changes of the [11 C]CFT binding to the striatal dopamine transporters in the Fischer 344 rats: a PET study. Ann Nucl Med. 2003;17:249–53. https://doi.org/10.1007/BF02990030.

50. Sawle GV, Colebatch JG, Shah A, Brooks DJ, Marsden CD, Frackowiak RS. Striatal function in normal aging: implications for Parkinson's disease. Ann Neurol. 1990;28:799–804. https://doi.org/10.1002/ana.410280611.

51. Wang Y, Li E, Cherry SR, Wang G, Total-Body PET. Kinetic modeling and potential opportunities using deep learning. PET Clin. 2021;16:613–25. https://doi.org/10.1016/j.cpet.2021.06.009.